Mesh adaptation driven by truncation error estimates

François Fraysse⋆*, Gonzalo Rubio*⋆ *and Eusebio Valero*⋆
⋆*Universidad Politécnica de Madrid*
E.T.S.I.Aeronáuticos, Applied Mathematics Department, Madrid, Spain

Abstract

In the present investigation, a mesh refinement method based on estimation of truncation error is presented and compared against feature-based adaptation strategy. The τ-estimation method uses auxiliary coarser meshes to estimate the local truncation error which can be used for driving an adaptation algorithm. The method is demonstrated in the context of 2d NACA0012 inviscid flow at subsonic regimes, where typical force coefficients are computed and compared.

1. Introduction

It has been shown that the CFD accuracy depends mainly on discretization errors for standard airplane at cruise conditions [16]. It is well known that discretization errors, in the asymptotic range, are dependent on the local size of the mesh as $O(h^p)$, where h represents the local size of the mesh elements and p the formal discretization order of the numerical method. The reduction of numerical errors may be accomplished by a twofold strategy: to increase the order of the discretization scheme and/or to increase the number of nodes. These two techniques are known as p- and h-adaptation respectively. In case of h-adaptation, the selection of a reliable adaptation parameter is a key aspect in order to reduce the errors in the computation. Adaptation parameters based on physical features work generally well when one aims at solving the details of the flow or improve the accuracy in regions where the physical scales must be resolved (shear layers, shock waves, etc.). However, it has been shown that increasing the resolution in these regions does not necessarily improve the accuracy of engineering outputs of interest as, for example, global forces [19]. Therefore, in the last years special attention has been paid to indicators based on numerical errors.

Since the discretized equations represent approximations to the differential equation, the exact solution of the latter does not satisfy the difference equation. The imbalance, which is due to truncation of the Taylor series, is called truncation error (TE). Analysis of the truncation error can be done by deriving analytically the Taylor series expansions for a given numerical scheme [4, 5, 6]. However, the primary issue with this approach is the complexity of the related expressions, specially for multi-dimensional problems on arbitrary grids. The second drawback is the lack of generality, as the truncation error differs from one numerical scheme to another. Another family of methods employed to study the discretization or truncation error are based on Richardson extrapolation [7, 8, 3]. The estimation of the discretization error by Richardson extrapolation [9, 10, 11] is based on the existence of a Taylor series expansion of the solution, assuming a smooth solution of the Partial Differential Equation (PDE). The major advantage of this approach is that it is independent of the numerical scheme, then easily extendable to any numerical solver. However, it requires the computation of an approximated solution on at least two meshes (three if the order of accuracy of the numerical scheme is considered as an unknown) of different spacings, making it hardly suitable for three-dimensional industrial applications.

On the other hand, the estimation of the truncation error by means of τ-estimation [3] is an interesting alternative as it does not require the solution on a secondary grid, but only the computation of the residual. Furthermore, it is closely linked to the forcing term in the Full Approximation Storage (FAS) approach of the multigrid technique [8], making it easy to compute in a solver where a multigrid strategy is implemented. Extensive analysis can be found in Bernert [12] and Fulton [13] on the accuracy of the estimation of the truncation error by τ-estimation, yielding stringent conditions on the restriction operators for transfers from fine-to-coarse/coarse-to-fine grids. Additionally, Fraysse et al [1] extend previous studies to more complex geometries and show the differences between finite difference and finite volume schemes.

Once a good estimation of the error is available, a robust mesh adaptation strategy can be derived. We propose in this paper to compare two mesh adaptation techniques: one based on flow features and one on the distribution of the local truncation error.

2. Error indicator by τ-estimation method

Let us consider the discretization of a PDE on a grid Ω_h indexed by a mesh size parameter h:

$$\mathbf{R}_h(\mathbf{U}_h) = 0$$

The corresponding local truncation error is defined as

$$\mathbf{R}_h(\mathbf{I}^h\mathbf{U}) = \tau^h \tag{1}$$

where $\mathbf{I}^h$ represents a linear continuum-to-grid Ω^h transfer for the exact solution $\mathbf{U}$. Therefore, the TE τ^h can be seen as the residual left by the exact solution when applied onto the discretized PDE.

In addition to the discrete equation Eq. 1, and considering a FAS multigrid algorithm [3], the coarse-grid equation may be written as

$$\mathbf{R}_H\hat{\mathbf{U}}_H = \mathbf{R}_H(\hat{\mathbf{I}}_h^H\widetilde{\mathbf{U}}_h) - \mathbf{I}_h^H(\mathbf{R}_h\widetilde{\mathbf{U}}_h), \qquad \hat{\mathbf{U}}_H = \hat{\mathbf{I}}_h^H(\epsilon_{it}^h + \widetilde{\mathbf{U}}_h) \tag{2}$$

corresponding to the discrete equation on a coarser mesh Ω^H, with mesh ratio $\rho = h/H < 1$. In Eq.2, $\widetilde{\mathbf{U}}_h$ is the current approximation of the solution (relaxed on the fine grid and not necessarily converged), $\epsilon_{it}^h = \mathbf{U}_h - \widetilde{\mathbf{U}}_h$ is the fine grid iteration error whose high frequencies are to be smoothed, $\hat{\mathbf{I}}_h^H$ represents the fine-to-coarse transfer operator of the solution whereas $\mathbf{I}_h^H$ represents the fine-to-coarse transfer operator of the residual. Similarly, introducing the *relative local truncation error* τ_h^H, Eq.2 may be written as

$$\mathbf{R}_H\hat{\mathbf{U}}_H = \tau_h^H \tag{3}$$

$$\tau_h^H = \mathbf{R}_H(\hat{\mathbf{I}}_h^H\widetilde{\mathbf{U}}_h) - \mathbf{I}_h^H(\mathbf{R}_h\widetilde{\mathbf{U}}_h) \tag{4}$$

Furthermore, as in this investigation we consider a converged solution, then τ_h^H reduces to

$$\tau_h^H = \mathbf{R}_H(\hat{\mathbf{I}}_h^H\mathbf{U}_h) \tag{5}$$

Our goal is to use τ_h^H to estimate τ^H. If this can be done with sufficient accuracy, then one can use this local error as a mesh adaptation indicator, uncertainty estimator or to increase the order of accuracy of the spatial scheme.

The following theorem provides the relation between the accuracy of τ_h^H towards τ^H and the order of the restriction operators acting in Eq.5.

Theorem 1 (Truncation Error Estimate) *Assume that there exists $p, n \geq 1$ and $q, s \geq 1$ such that if $\mathbf{U} \in C^{n+p+q}(\Omega)$, the truncation error (1) satisfies:*

- ***(A1)** Local truncation error of order p: $\tau^h = h^p\mathbf{I}^h\mathbf{V} + O(h^{p+q}), \quad \mathbf{V} \in C^q$*
- ***(A2)** Local discretization error of order p: $\epsilon^h = h^p\mathbf{I}^h\mathbf{W} + O(h^{p+q}), \quad \mathbf{W} \in C^q$*
- ***(A3)** Fine-to-coarse transfer operator of the solution of order s: $\hat{\mathbf{I}}_h^H\mathbf{I}^h\mathbf{U} = \mathbf{I}^H\mathbf{U} + O(h^s)$*

  then

$$\tau_h^H = (1 - \rho^p)\tau^H + O(h^{min(s,p+q,2p)}), \qquad \rho = h/H. \tag{6}$$

The main conclusion of Eq.6 is related with the order of the restriction operator s of the solution. Looking at the exponent of the order of magnitude of the remaining term in Eq.6, it can be deduced that it is necessary to use higher order interpolation $s > p$ to transfer the solution from fine to coarse mesh. If $s \leq p$ then the TE estimation will be dominated by a term $O(h^s)$, spoiling the general results of the formula. Proofs to this theorem, together with a detailed analysis of the TE in general geometries and schemes can be found in Fraysse et al [1, 2].

Our aim in this work is to test the capabilities of a mesh adaptation algorithm, driven by TE distribution, to improve the accuracy of engineering functional outputs. So this study will focus on *a posteriori* adaptation of steady flows. Furthermore, as it will be detailed later, the coarse grid employed for the computation of the TE estimate, on which the fine grid solution is restricted, is built in such a way that each fine grid nodes coincide to a coarse grid node. In this way, no complex restriction operator has to be considered to recover full accuracy of the estimator, direct injection can be performed like in a finite differences formulation.

3. Mesh adaptation methodology

The methods described here have been implemented and checked in the industrial DLR TAU-Code [15]. In TAU, adaptation is performed by bisecting the edges of an element according to some specific sensor. In this section, we will describe the adaptation algorithms based either flow feature and on the TE estimation.

3.1 Feature-based adaptation methodology

A widely used mesh adaptation method is based on local physical sensors. This method is usually known as the feature-based sensor.

In order to select zones to be refined, it is first determined which edges of the primary grid have to be adapted depending on the desired dimensions for the resulting grid.

Thus, for all edges an adaptation parameter I_f is defined. Only the edges above some specific threshold are bisected. I_f is defined as:

$$I_f = \Delta V_e ||\mathbf{x}_e||_2^{\alpha},$$

where $||\cdot||_2$ is the usual Euclidean norm, $\mathbf{x}_e = \mathbf{x}_{p_1} - \mathbf{x}_{p_2}$ is the vector edge, α an edge length scaling factor, typically set to $\alpha = 0.5$, and

$$\Delta V_e = \max\left(c_{\phi_i}\frac{\Delta\phi_i}{(\Delta\phi_i)_{max}}\right), \qquad \text{with } 0 \leq i < N,$$

N being the number of different flow variables considered. In this study, ϕ_i is an equal combination of density, velocity module, total enthalpy and total pressure. Thus:

$$\Delta\phi_i = |\phi_i(\mathbf{x}_{p_1}) - \phi_i(\mathbf{x}_{p_2})|.$$

The weights c_{ϕ_i} are parameters enabling to choose different combinations of the single parts of the indicator.

Finally, for an equilibrated scaling of each part the calculated values must be distributed in $[0, 1]$. Therefore, the maximum of all values is determined by

$$(\Delta\phi_i)_{max} = \max\left((\Delta\phi_i)_e\right). \qquad \text{for all edges } e$$

3.2 Truncation error-based adaptation methodology

In order to compute an accurate estimation of the local TE, it is necessary to dispose of two grids, which are topologically consistent [1]. For that purpose, we denote the coarse grid by Ω^H and the fine grid by Ω^h (which is the actual grid where the flow is solved) obtained by uniform refinement of grid Ω^H. Constructing the fine grid Ω^h from the coarse grid Ω^H gives two major advantages in the scope of TE estimation: on the one hand, the conservation of grid characteristics (non-uniformities, distortion, etc) ensuring that the computed error on Ω^H is truly representative of the error on Ω^h; on the second hand, each fine grid point coincides with a coarse grid point, which avoids to implement a high order restriction of the fine grid solution onto the coarse grid.

Thus, following Eq.5, the TE-based sensor developed in this work is defined as:

$$I_{te_i} = \frac{|\Omega_i^H|^{\alpha}}{1-\rho^p}\left|\tau_{h_i}^H\right|, \quad i \text{ node index} \tag{7}$$

where

- $|\Omega_i^H|$ is the volume of the element associated to node i. This scaling prevents to perform infinite refinements in regions where the error might decrease at a very low rate (typically, shock waves) without substantially contribute to the prescribed functional.
- α is an edge length scaling factor, set here to $\alpha = 0.5$.
- $\rho = h/H$ is a characteristic grid length ratio from grid Ω^h to grid Ω^H, set here to $\rho = 0.5$.
- p is the formal order of accuracy set to $p = 2$ using the Jameson-Schmidt-Turkel (JST) spatial scheme.
- $\tau_{h_i}^H$ is the TE at node i, obtained by applying Eq.5.

$$\tau_{h_i}^H = \mathbf{R}_{h_i}^q \left(\hat{\mathbf{I}}_h^H \mathbf{U}_{h_i}\right)$$

  where $\mathbf{R}_q^{h_i}$ is the residual associated to the equation q (density, momentum or total energy). In these computations the TE associated with the density $q = 1$ has been considered. No significant differences in the adapted meshes have been observed if the momentum or energy equations are considered in the computation of the sensor.
- $\hat{\mathbf{I}}_h^H$ is a restriction operator from grid Ω^h to grid Ω^H. As explained earlier, the way we contruct Ω_h and Ω_H allows the use of direct injection ($s = \infty$).
- $\mathbf{U}_h$ is the converged solution obtained on grid Ω^h.

  A point i on the grid Ω^H is then flagged for refinement if

$$I_{te_i} \geq \lambda$$

where λ is a user-given threshold which controls the trade-off between increased accuracy and increased work. Typical values of this parameter are $O(h^3)$.

Based on this indicator strategy, one cycle of adaptation is performed in this way:

1. Solution $\mathbf{U}_h$ of the primal equations on grid Ω^h.
2. Pointwise restriction of the solution $\mathbf{U}_h$ from grid Ω^h to grid Ω^H.
3. Computation of the TE-based sensor of Eq. 7 on grid Ω^H.
4. Laplacian smoothing of the TE-based sensor
5. Output of a file containing the indices of the nodes of grid Ω^H where the indicator is above the user-given threshold λ.
6. Full refinement of all elements sharing a marked node on grid Ω^H.
7. Uniform refinement of grid $\Omega^{H_{ad}}$ to grid $\Omega^{h_{ad}}$.

A key point of this procedure is that the adaptation is performed on the coarse grid Ω^H. Then the final adapted grid $\Omega^{h_{ad}}$ is obtained by global refinement of grid $\Omega^{H_{ad}}$. This choice ensures that the two grid levels generated are topologically consistent, which allows to compute again the TE for a further adaptation cycle, thus avoiding an extra source of error due to inconsistency between meshes.

4. Numerical results

4.1 Introduction

A brief analysis on the truncation error-based adaptation in one dimension is introduced in this section. The following problem has been considered:

$$-u''(x) = f(x) + bc, \quad \forall x \in \Omega = [-4, 4] \tag{8}$$

where *bc* stands for boundary conditions. And we consider the following test function:

$$\begin{cases} f(x) = -4\dfrac{\sinh(x)}{\cosh(x)} \\ \\ u(-4) = u_{ex}(-4), \quad u(4) = u_{ex}(4) \end{cases} \tag{9}$$

This problem has the exact solution

$$u_{ex}(x) = -2\frac{\sinh(x)}{\cosh(x)}$$

The aim of this preliminary work is to see how the truncation error might affect the global accuracy. To do so, with an exact solution in hand, the exact truncation error can be extracted by injecting the exact solution into the numerical scheme (Eq.1). Then a simple redistribution/mesh enrichment algorithm has been developped and applied to the problem of Eq.8. Eq.8 is numerically solved using second order centered finite differences on an initial uniform grid composed of only 5 points (see Fig.1(a)). Then the adaptation algorithm tries to redistribute/enrich the mesh until a prescribed maximum value $\tau_{max} = 0.001$ over the domain Ω^h is obtained, which represents a drop of more than two orders of magnitude. In this case the final mesh is composed of 301 nodes (see Fig.1(b)).

In Fig.1(e)-(f) are reported the values of the truncation error and the discretization error, for the initial grid and the TE-based adapted grid. The results are compared against uniform refinement. Both truncation error and discretization error reduce at a higher rate than global refinement. This very simple test shows the importance of the truncation error in the accuracy of numerical solutions. The truncation error acts as a source term for the discretization error (through the so-called Discretization Error Transport Equation), and its accurate evaluation can give valuable information, in particular for mesh adaptation.

In order to test and compare the adaptation techniques presented in the last sections, we will present in the following a two-dimensional test case representative more representative of indistrial applications.

The two-dimensional test case considered here will be computed on a NACA0012 airfoil at subsonic free stream conditions. Results on this profile have been reported previously in the context of feature-based [17], adjoint-based [14] and residual-based [18] grid adaptation. The results of TE-based adaptation will be compared against the common feature-based adaptation technique. The latter is an equal combination of density, velocity module, total enthalpy and total pressure. The adaptation using feature-based approach is driven by a fixed percentage of new added point, here set to 40%. We will present a study of the evolution of the force coefficients (namely lift, and y-moment) with respect to the number of nodes for the two adaptation techniques discussed earlier.

4.2 Inviscid subsonic 2D test case

The initial grid is composed of 11750 nodes, 23040 triangles and 459 points on the airfoil. The outer boundary is located at a distance of 50 chords away from the airfoil profile. This initial grid is obtained by global refinement of an initial coarse mesh. The existence of both meshes is necessary in order to start the TE-based adaptive process described in Sec. 3. The farfield conditions imposed are $M_\infty = 0.4$ and $\alpha = 5°$, which yields a fully subsonic steady solution.

Two different functionals are analyzed in this case: the lift (C_L) and y-moment (C_{M_y}). For the TE and feature-based estimators, the sensors for both functionals are based on density and an equally balanced combination of density, velocity module, total pressure and enthalpy respectively. A threshold $\lambda = 0.0001$ has been in the TE-based adaptation algorithm.

The adapted meshes are presented in Fig.2 after four cycles of adaptation. The two methods clearly create different meshes. The TE-based indicator creates a mesh which is highly refined at the leading edge and at the trailing edge. As far as the feature-based adaptation procedure is concerned, it refines more uniformly around the profile and specially in the region where the flow accelerates (on the suction side close to the leading edge). Note that the differences in the extension of the adapted areas are significant, specially for the feature-based method, for which a large area of the suction side is adapted.

Finally, in Fig.3 the C_L and C_{M_y} coefficients have been computed at each adaptation cycle for the two methodologies and compared against uniform refinement and the value obtained by Richardson extrapolation. The two adaptation indicators yield an improved prediction of C_L and C_{M_y} with respect to the initial mesh. The two methods allow a rapid convergence of C_L and C_{M_y}. The TE-based permits a gain of more than an order of magnitude in the number of nodes with respect to uniform refinement, and yield comparable or better levels of functional outputs as the feature-based approach but with fewer points.

5. Conclusions

Decreasing computational work by mesh adaptation has been proven an elegant and efficient technique. However, current formulations employing indicators for mesh (de-)refinement based on flow features do not take into account the hyperbolic properties of Euler equations, and no guarantee can be given on the convergence of the adaptation procedure to the uniform refinement procedure. Furthermore, adapting the grid based on flow variables will not necessarily improve the accuracy of global quantities of interest in industry, such the lift or drag values.

This leads to the development of adaptation algorithms based on numerical error. In this work a TE-based indicator has been successfully developed and showed better convergence properties of force coefficients on 2d Euler testcases than feature based sensors.

References

[1] Fraysse F., de Vicente, J. and Valero, E., *The estimation of truncation error by τ-estimation revisited*, Journal of Computational Physics, under revision

[2] Fraysse F., de Vicente, J. and Valero, E., *Extension of τ-estimation to finite volumes solvers*, V International Conference on Adaptive Modeling and Simulation, ADMOS 2011

[3] Brandt, A., *Multigrid Techniques: 1984 Guide with applications to fluid dynamics*

[4] Leonard, B. P., *Comparison of Truncation Error of Finite-Difference and Finite-Volume Formulations of Convection Terms*, NASA Technical Memorandum 105861, ICOMP-92-19, September 1992

[5] Jeng, Y. N. and Chen, J. L., *Truncation Error Analysis of the Finite Volume Method for Steady Convective Equation*, Journal of Computational Physics, 100, pp. 64-76, 1992

[6] Hagen, S. F., *Estimation of the Truncation Error for the Linearized, Shallow Water Momentum Equations*, Engineering with Computers, 17, pp. 354-362, 2001

[7] Briggs, W., Henson, V. E. and S. McCormick, S.,*A Multigrid Tutorial*, Second ed., Society for Industrial and Applied Mathematics, Philadelphia, PA, 2000

[8] Trottenberg, U., Oosterlee, C. and Schüler, A., *Multigrid*, Academic Press

[9] Ilinca, C., Zhang, X. D., Trépanier, J.-Y. and Camarero, R., *A comparison of three error estimation techniques for finite-volume solutions of compressible flows*, Comput. Methods Appl. Mech. Engrg., 189, pp. 1277-1294, 2000

[10] Garbey, M. and Shyy, W., *Error Estimation, Multilevel Method and Robust Extrapolation in the Numerical Solution of PDEs*, Fourteenth International Conference on Domain Decomposition Methods

[11] Phillips, T. S. and Roy, C., *Evaluation of Extrapolation-Based Discretization Error and Uncertainty Estimators*, 49th AIAA Aerospace Science Meeting, AIAA 2011-215

[12] Bernert, K. *τ-Extrapolation-Theoretical foundation, numerical experiment, and application to Navier-Stokes equations* SIAM J. Sci. Comput. Vol. 18, No. 2, pp. 460-478, March 1997

[13] Fulton, S. R. *On the accuracy of multigrid truncation error estimates* Electronic transactions on numerical analysis, Vol. 15, pp 29-37, 2003

[14] Venditti, D. A., *Grid Adaptation for Functional Outputs of Compressible Flow Simula- tions*, Ph.D. thesis, Massachusetts Institute of Technology, Cambridge, MA, 2002

[15] Technical Documentation of the DLR TAU-code. Release 20010.1.0. March 2010

[16] Mavriplis, D. J., *Grid Resolution Study of a Drag Prediction Workshop Configuration using NSU3D Unstructured Mesh Solver*, AIAA Paper 2005-4729, 2005

[17] Warren, G. P., Anderson, W. K., Thomas, J. P., Krist, S. L.,*Grid Convergence for Adaptive Methods*, AIAA Paper 91-1592, 1991

[18] Zhang, X. D., Vallet, M-G., Trepanier, G-Y, Camarero, R., Lassaline, J., Manzano, L. M., Zingg, D.,*Mesh Adaptation Using Different Error Indicators for the Euler Equations*, 15th AIAA Computational Fluid Dynamics Conference, AIAA-2549, 2001

[19] Balasubramanian, R., Newman, J. C., *Comparison of Adjoint-based and Feature-based Grid Adaptation for Functional Outputs*, 24th AIAA Applied Aerodynamics Conference, AIAA 2006-3314, 2006

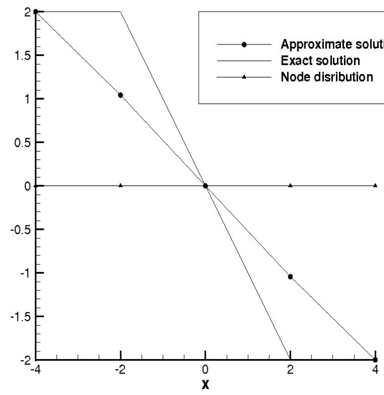

(a)

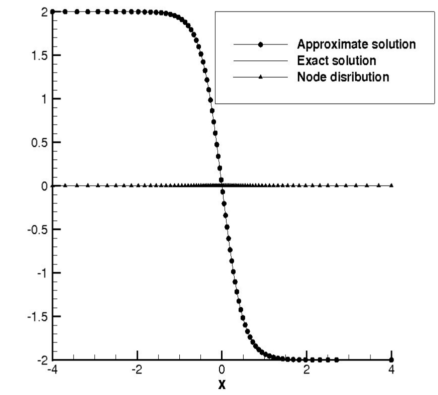

(b)

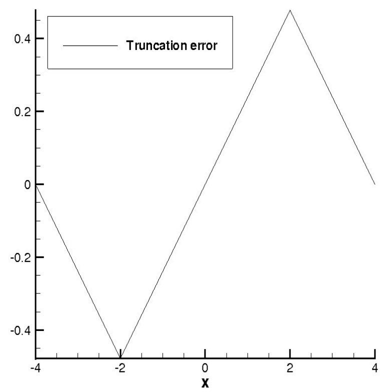

(c)

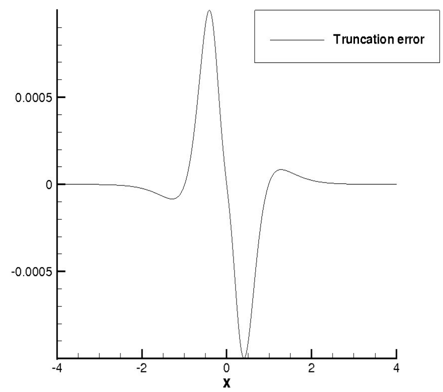

(d)

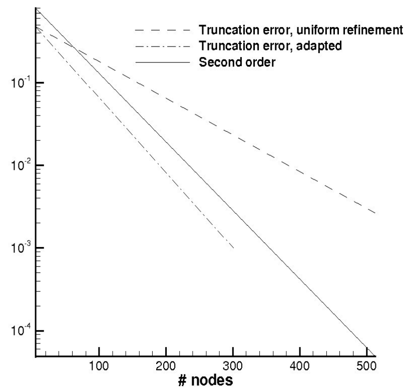

(e)

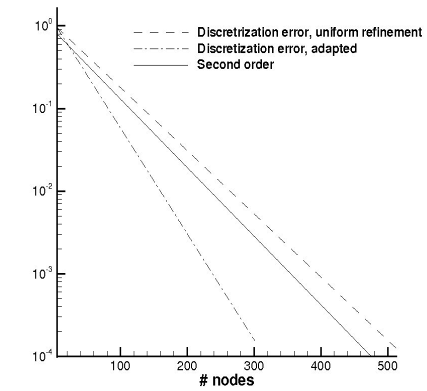

(f)

Figure 1: 1D Poisson equation. (a) initial mesh (5 nodes), (b) final mesh (301 nodes), (c) TE distribution initial mesh, (d) TE distribution final mesh, (e) TE-magnitude, (d) discretization error magnitude

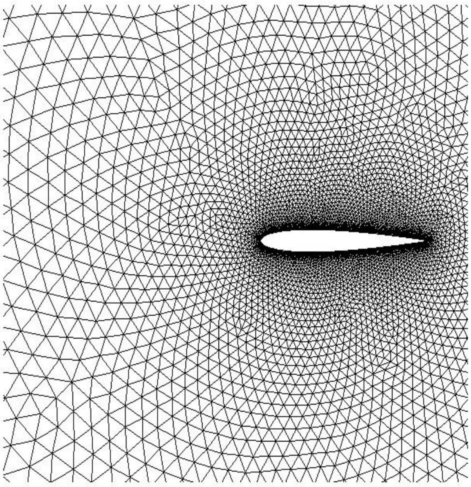

(a)

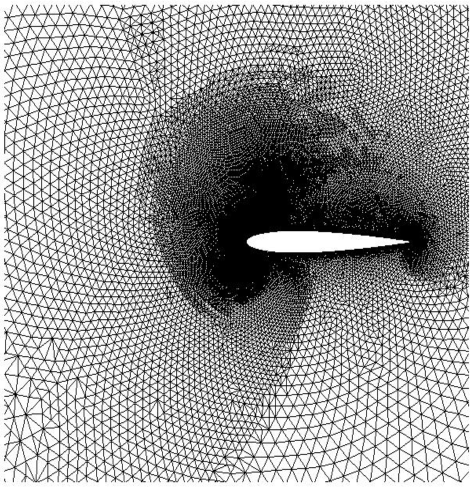

(b)

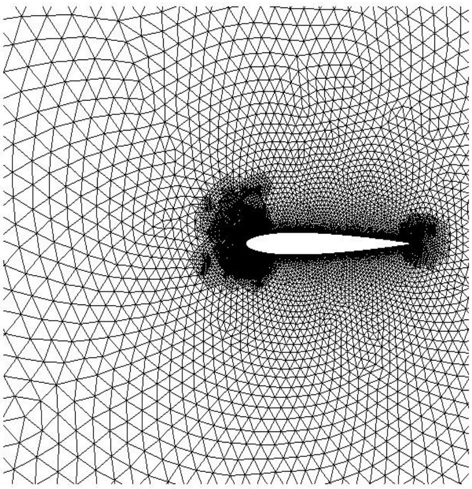

(c)

Figure 2: NACA0012 grids, $M_\infty = 0.4, \alpha = 5^\circ$. (a) initial mesh (11750 nodes), (b) 4 feature-based adaptation cycles (45214 nodes), (c) 4 TE-based adaptation cycles (40211 nodes)

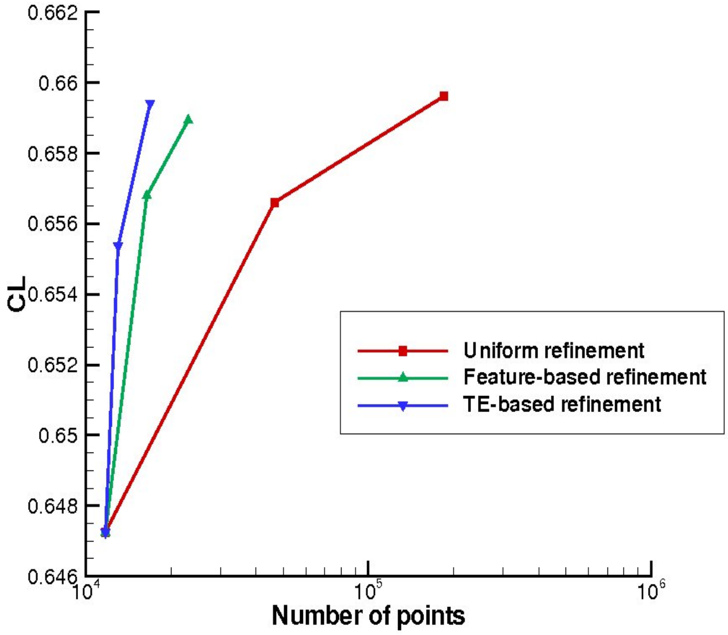

(a)

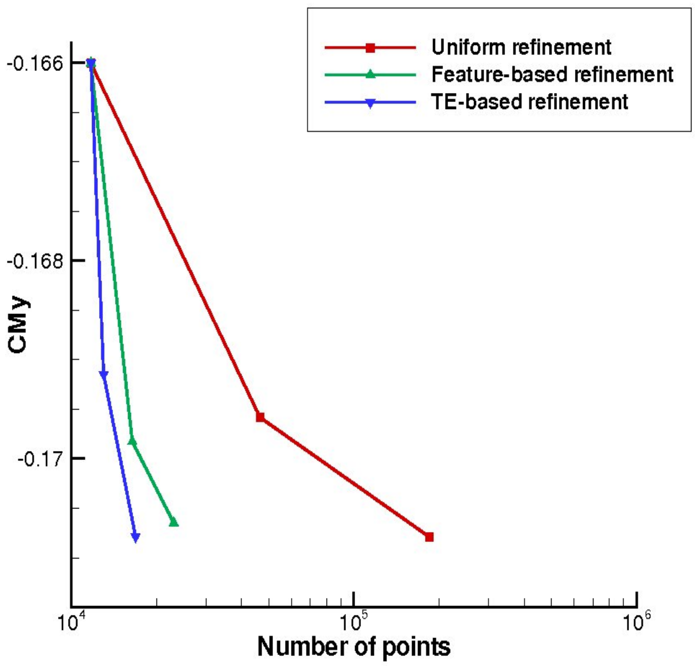

(b)

Figure 3: NACA 0012 convergence of force coefficients, $M_\infty = 0.4, \alpha = 5°$. (a) C_L, (b) CM_y